Physics Letters B 788 (2019) 42–51

Contents lists available at ScienceDirect

Physics Letters B

www.elsevier.com/locate/physletb

Precise measurement of R_{uds} and R between 1.84 and 3.72 GeV at the KEDR detector

V.V. Anashin [a], O.V. Anchugov [a], V.M. Aulchenko [a,b], E.M. Baldin [a,b], G.N. Baranov [a,c], A.K. Barladyan [a], A.Yu. Barnyakov [a,b], M.Yu. Barnyakov [a,b], S.E. Baru [a,b], I.Yu. Basok [a], A.M. Batrakov [a], E.A. Bekhtenev [a], A.E. Blinov [a,b], V.E. Blinov [a,b,c], A.V. Bobrov [a,b], V.S. Bobrovnikov [a,b], A.V. Bogomyagkov [a,b], A.E. Bondar [a,b], A.R. Buzykaev [a,b], P.B. Cheblakov [a,b], V.L. Dorohov [a,c], S.I. Eidelman [a,b], D.N. Grigoriev [a,b,c], S.A. Glukhov [a], V.V. Kaminskiy [a], S.E. Karnaev [a], G.V. Karpov [a], S.V. Karpov [a], K.Yu. Karukina [a,c], D.P. Kashtankin [a], P.V. Kasyanenko [a], T.A. Kharlamova [a], V.A. Kiselev [a], V.V. Kolmogorov [a], S.A. Kononov [a,b], K.Yu. Kotov [a], A.A. Krasnov [a], E.A. Kravchenko [a,b], V.N. Kudryavtsev [a,b], V.F. Kulikov [a,b], G.Ya. Kurkin [a,c], I.A. Kuyanov [a], E.B. Levichev [a,c], D.A. Maksimov [a,b], V.M. Malyshev [a], A.L. Maslennikov [a,b], O.I. Meshkov [a,b], S.I. Mishnev [a], I.A. Morozov [a], I.I. Morozov [a,b], S.A. Nikitin [a], I.B. Nikolaev [a,b], I.N. Okunev [a], A.P. Onuchin [a,b,c], S.B. Oreshkin [a], A.A. Osipov [a,b], I.V. Ovtin [a,c], S.V. Peleganchuk [a,b], S.G. Pivovarov [a,c], P.A. Piminov [a], V.V. Petrov [a], V.G. Prisekin [a,b], O.L. Rezanova [a,b], A.A. Ruban [a,b], G.A. Savinov [a], A.G. Shamov [a,b], D.N. Shatilov [a], D.A. Shvedov [a], B.A. Shwartz [a,b], E.A. Simonov [a], S.V. Sinyatkin [a], A.N. Skrinsky [a], A.V. Sokolov [a,b], D.P. Sukhanov [a], A.M. Sukharev [a,b], E.V. Starostina [a,b], A.A. Talyshev [a,b], V.A. Tayursky [a,b], V.I. Telnov [a,b], Yu.A. Tikhonov [a,b], K.Yu. Todyshev [a,b,*], A.G. Tribendis [a], G.M. Tumaikin [a], Yu.V. Usov [a], A.I. Vorobiov [a], V.N. Zhilich [a,b], A.A. Zhukov [a], V.V. Zhulanov [a,b], A.N. Zhuravlev [a,b]

[a] *Budker Institute of Nuclear Physics, 11, akademika Lavrentieva prospect, Novosibirsk, 630090, Russia*
[b] *Novosibirsk State University, 2, Pirogova street, Novosibirsk, 630090, Russia*
[c] *Novosibirsk State Technical University, 20, Karl Marx prospect, Novosibirsk, 630092, Russia*

ARTICLE INFO

Article history:
Received 17 May 2018
Received in revised form 16 October 2018
Accepted 7 November 2018
Available online 12 November 2018
Editor: M. Doser

ABSTRACT

The present work continues a series of the KEDR measurements of the R value that started in 2010 at the VEPP-4M e^+e^- collider. By combining new data with our previous results in this energy range we measured the values of R_{uds} and R at nine center-of-mass energies between 3.08 and 3.72 GeV. The total accuracy is about or better than 2.6% at most of energy points with a systematic uncertainty of about 1.9%. Together with the previous precise R measurement at KEDR in the energy range 1.84–3.05 GeV, it constitutes the most detailed high-precision R measurement near the charmonium production threshold.

1. Introduction

The ratio of the radiatively corrected total cross section of electron-positron annihilation into hadrons to the lowest-order QED cross section of the muon pair production is referred to as the value of R. This quantity plays critical role in various precision tests of the Standard Model, e.g. $R(s)$ measurements are employed to determine the hadronic contribution to the anomalous magnetic moment of the muon and the value of the electromagnetic fine structure constant at the Z^0 peak $\alpha(M_Z^2)$ [1,2], the running strong coupling constant $\alpha_s(s)$ and heavy quark masses [3].

* Corresponding author at: Budker Institute of Nuclear Physics, 11, akademika Lavrentieva prospect, Novosibirsk, 630090, Russia.
E-mail address: todyshev@inp.nsk.su (K.Yu. Todyshev).

https://doi.org/10.1016/j.physletb.2018.11.012

Table 1
Center-of-mass energy $\sqrt{s}$ and integrated luminosity $\int \mathcal{L}dt$.

Point	$\sqrt{s}$, MeV	$\int \mathcal{L}dt$, nb^{-1}
1	3076.7 ± 0.2	$103.45 \pm 0.98 \pm 0.93$
2	3119.2 ± 0.2	$77.15 \pm 0.86 \pm 0.69$
3	3221.8 ± 0.2	$93.18 \pm 0.98 \pm 0.84$
4	3314.7 ± 0.4	$157.69 \pm 1.31 \pm 1.42$
5	3418.3 ± 0.8	$150.46 \pm 1.33 \pm 1.35$
6	3499.6 ± 1.1	$125.76 \pm 1.23 \pm 1.13$
7	3618.1 ± 0.4	$159.97 \pm 1.43 \pm 1.44$
8	3719.6 ± 0.2	$130.90 \pm 1.34 \pm 1.18$

More than ten experiments contributed to the $R(s)$ measurement in the energy range between the $p\bar{p}$ and $D\bar{D}$ thresholds [4–16]. The most accurate results were obtained in the experiments of BES-II [14] and KEDR [15,16], in which the accuracy of about 3.3% was reached at separate points.

For the considered energy range, systematic uncertainties give a substantial contribution to the total accuracy of the $R(s)$ quantity. This fact motivated us to repeat the R measurement in the given energy range after repairing and upgrading the detector. In 2014 the region of the J/ψ and $\psi(2S)$ resonances was scanned in the KEDR experiment with an integrated luminosity of about 1.3 pb^{-1}.

2. Experiment

The experiment was carried out at the VEPP-4M [17] collider in the same approach that was used earlier in [15].

The KEDR detector and its performance are described in detail elsewhere [18]. At the end of 2013, the repair and upgrade of the detector were completed. The vacuum chamber was replaced with a new wider one to reduce possible accelerator background. The preamplifiers of the VD were reconfigured and equipped with additional copper-foil screens to suppress the crosstalk. The drift chamber was renovated and a few layers were repaired. A second layer of the aerogel Cherenkov counters was installed. The barrel part of the TOF system was equipped with additional magnetic shields to suppress the reduction of signal amplitudes in photomultipliers in the magnetic field. The entire krypton was cleaned of electronegative impurities.

The purpose of the experiment was to repeat the R scan carried out by KEDR in 2011, in addition we collected data at the energy point below the J/ψ. The total hadronic cross section was measured at eight points between 3.08 and 3.72 GeV. The value of energy was calculated by interpolating the resonance depolarization results obtained in calibration runs.

The actual energies and the integrated luminosity at the points are presented in Table 1. To determine resonance parameters additional data samples of about 0.34 pb^{-1} were taken in the vicinity of the J/ψ and $\psi(2S)$ resonances. A measurement of beam energy by the resonance depolarization method was carried out at least once at each listed point off the resonance peak regions. The assigned energy errors are due to the drift of the parameters of the accelerator during data taking. The data points and the resonance fits are shown in Fig. 1.

3. Data analysis

3.1. Analysis procedure

Details of the analysis procedure are provided in [15].

To determine the R value we take into account narrow resonances explicitly instead of including them in the radiative correction $\delta(s)$. The narrow-resonance cross section depends on the combination $\varepsilon_\psi \Gamma_{ee}\mathcal{B}_h$. The efficiencies ε_ψ were extracted by fitting the data at the resonance regions, thus the obtained resonance cross section is not sensitive to the world-average values of the leptonic width Γ_{ee} and the hadronic branching fraction $\mathcal{B}_h$ used. Computations of a narrow-resonance cross section, the resonance – continuum interference and the resonance fitting procedure are described in more detail in Refs. [19,20].

Table 2
Efficiency, energy spread and χ^2 probability of the fits of the J/ψ and $\psi(2S)$ resonances (statistical errors only are presented). The reference energy points for the energy spread parameters correspond to masses of the J/ψ and $\psi(2S)$ mesons taken from PDG [21].

	Efficiency, %	σ_W, MeV	$P(\chi^2)$, %
J/ψ	78.72 ± 0.89	0.785 ± 0.004	53.5
$\psi(2S)$	80.65 ± 1.95	1.262 ± 0.045	99.4

Table 3
Relative contribution of the J/ψ and $\psi(2S)$ resonances to the observed multihadronic cross section. Negative signs correspond to resonance – continuum interference.

Point	$\frac{\sigma_{J/\psi}}{\sigma_{\rm obs}}$, %	$\frac{\sigma_{\psi(2S)}}{\sigma_{\rm obs}}$, %
1	−7.24(interference)	
2	59.71	
3	22.63	
4	14.83	
5	10.75	
6	8.76	
7	6.80	−0.76(interference)
8	4.05	28.27

The floating parameters were the detection efficiency ε_ψ at the world-average values of the leptonic width Γ_{ee} and its product by the hadronic branching fraction $\mathcal{B}_h$, the machine energy spread and the magnitude of the continuum cross section observed at the reference point below the resonance. The J/ψ and $\psi(2S)$ detection efficiencies, the collision energy spreads obtained and the χ^2 probabilities of the fits are presented in Table 2.

Table 3 lists the relative contribution of the J/ψ and $\psi(2S)$ to the observed cross section.

The detection efficiencies for the single-photon annihilation to hadrons $\varepsilon(s)$ and background processes were obtained from simulation.

The radiative correction factor is determined by excluding a contribution of the J/ψ and $\psi(2S)$ resonances and can be written as

$$1+\delta(s) = \int \frac{dx}{1-x}\,\frac{\mathcal{F}(s,x)}{\left|1-\tilde{\Pi}((1-x)s)\right|^2}\,\frac{\tilde{R}((1-x)s)\,\varepsilon((1-x)s)}{R(s)\,\varepsilon(s)}, \tag{1}$$

where $\mathcal{F}(s,x)$ is the radiative correction kernel [22]. The variable x is a fraction of s lost due to the initial-state radiation. The vacuum polarization operator $\tilde{\Pi}$ and the quantity $\tilde{R}$ do not include a contribution of narrow resonances, details of the calculation are presented in Sec. 3.7.

Thus, we extract the $R_{\rm uds}$ value, then by adding the contribution of narrow resonances we obtain the quantity R.

3.2. Monte Carlo simulation

The KEDR simulation program is based on the GEANT package, version 3.21 [23].

To simulate single-photon annihilation to hadrons we employ the JETSET 7.4 code [24] with the parameters tuned at each energy point. As an alternative way of generating events of the uds continuum, we use the LUARLW generator [25].

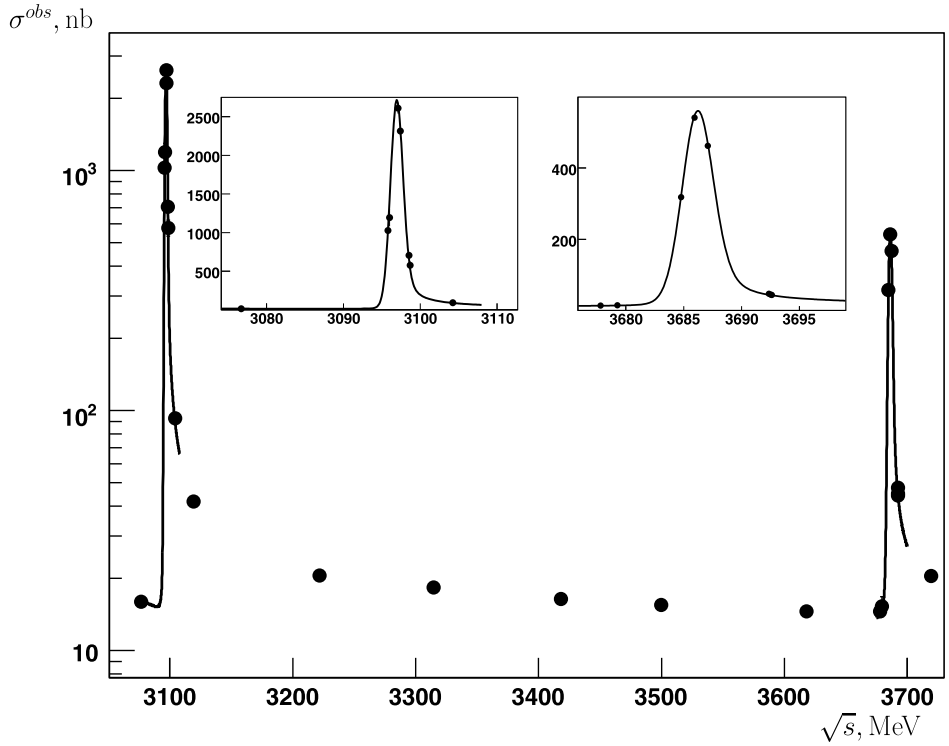

Fig. 1. The observed multihadronic cross section as a function of the c.m. energy for the two scans. The curves are the result of the fits of the narrow resonances. The insets show closeup of the J/ψ and $\psi(2S)$ regions.

Bhabha scattering events required for the precise luminosity determination are simulated by BHWIDE [26]. The MCGPJ generator [27] provides simulation of $\mu^+\mu^-$ events and the $e^+e^- \to e^+e^-\gamma$ process as an alternative to BHWIDE. The detection efficiency for $\tau^+\tau^-$ events was obtained using the KORALB event generator [28]. The two-photon processes $e^+e^- \to e^+e^-X$ are simulated with the generators described in Refs. [29–31].

The J/ψ and $\psi(2S)$ decays were simulated with the tuned version of the BES generator [32] based on the JETSET 7.4 code [19,33].

During the whole experiment random trigger events were recorded. These events were embedded into the Monte Carlo simulated data to account for various detector noises and a coincidence of the simulated processes with the collider and cosmic backgrounds.

Some important event characteristics are presented in Fig. 2, from which one can see that the experimental and simulated distributions agree rather well.

3.3. Event selection and detection efficiencies

In the offline analysis both experimental and simulated events pass the software event filter. By using a digitized response of the detector subsystems the software filter recalculates the PT and ST decisions with stringent conditions. This procedure reduces a systematic uncertainty due to trigger instabilities and uncertainties on the hardware thresholds.

To suppress the machine background to an acceptable level, the following PT conditions were used by OR:

- signals from $\geq$ two non-adjacent scintillation counters,
- signal from the LKr calorimeter,
- coincidence of the signals from two CsI endcaps.

Table 4
Selection criteria for hadronic events which were used by AND.

Variable	Allowed range
$N_{\text{particles}} \geq 3$ OR $\tilde{N}^{\text{IP}}_{\text{track}} \geq 2$	
$N^{\text{IP}}_{\text{track}}$	≥ 1
E_{obs}	> 1.6 GeV
$E^{\text{max}}_{\gamma}/E_{\text{beam}}$	< 0.82
E_{cal}	> 0.65 GeV
H_2/H_0	< 0.9
$\lvert P^{\text{miss}}_{z}/E_{\text{obs}}\rvert$	< 0.6
$E_{\text{LKr}}/E_{\text{cal}}$	> 0.15
$\lvert Z_{\text{vertex}}\rvert$	< 15.0 cm

Signals from two particles with the angular separation $\gtrsim 20°$ should satisfy numerous ST conditions.

The MC simulation shows that the trigger efficiency for continuum uds production increases from 96.2% at 3.08 GeV to 98.0% at 3.72 GeV.

Selection criteria for multihadronic events are presented in Table 4 and their description is given below. Here N^{IP}_{track} is the number of tracks originated from the interaction region defined as: $\rho < 5$ mm, $|z_0| < 130$ mm, where ρ is the track impact parameter relative to the beam axis and z_0 – the coordinate of the closest approach point. The $\tilde{N}^{IP}_{track}$ is the number of tracks satisfying the conditions above with E/p less than 0.6, where E/p means the ratio of the energy deposited in the calorimeter to the measured momentum of the charged particle. The multiplicity $N_{\text{particles}}$ is a sum of the number of charged tracks and the number of neutral particles detected in the calorimeters.

The observable energy E_{obs} is defined as a sum of the photon energies measured in the electromagnetic calorimeter and charged particle energies computed from the track momenta by assuming pion masses. The observable energy cut and limitation on the ratio of the energy of the most energetic photon to the beam energy

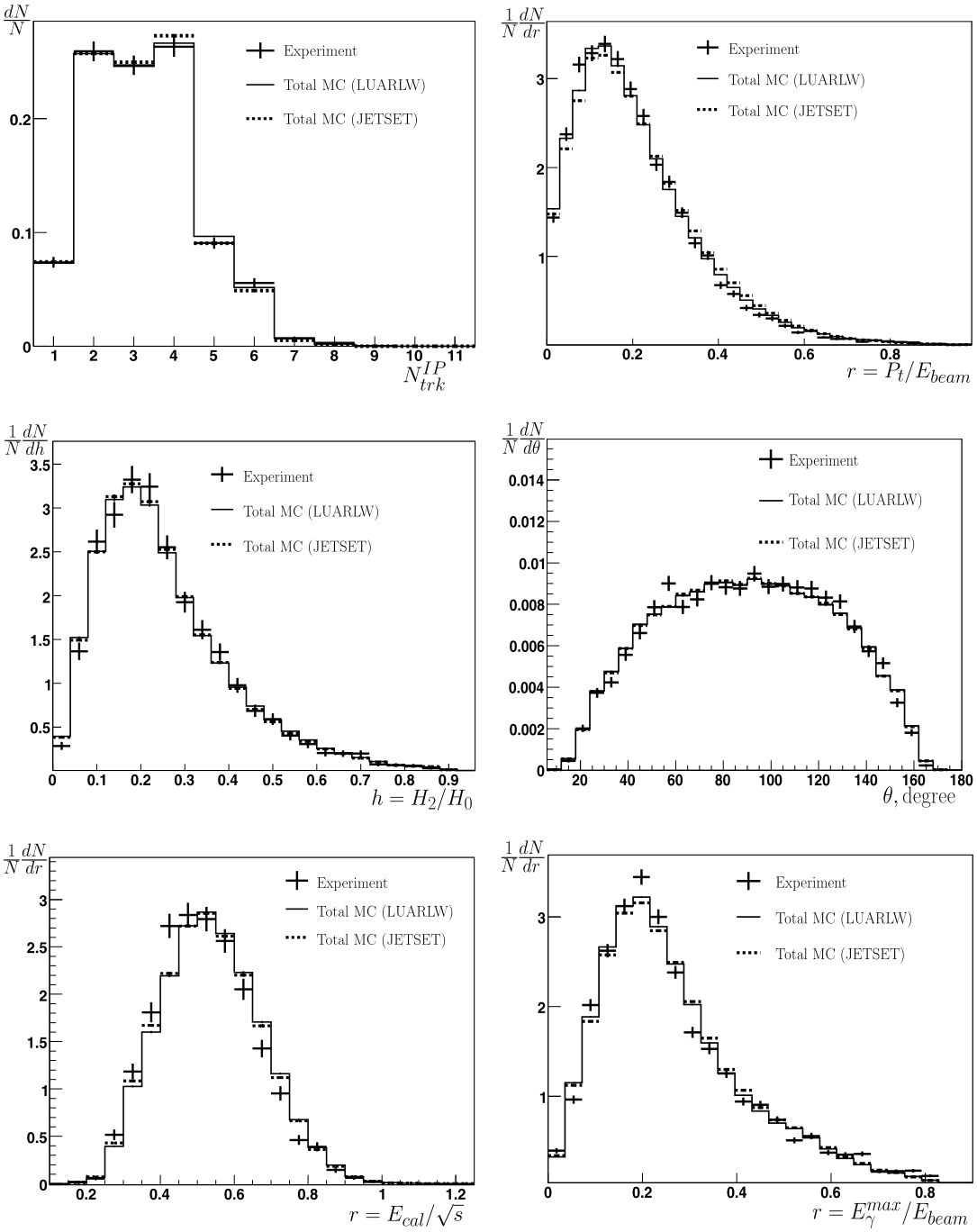

Fig. 2. Properties of hadronic events produced in the uds continuum at 3.119 GeV. Here N is the number of events, N_{trk}^{IP} is the number of tracks originating from the interaction region, P_t is a transverse momentum of the track, H_2 and H_0 are the Fox–Wolfram moments [34], θ is a polar angle of the track, $E_{\rm cal}$ is energy deposited in the calorimeter, $E_{\gamma}^{\rm max}$ is energy of the most energetic photon. The experimental distribution and two variants of MC simulation based on LUARLW and JETSET are plotted. Total MC includes simulation of the uds continuum, contributions of the narrow resonances and leptonic channels, we also added the contribution of residual machine background obtained from experimental runs with separated electron and positron beams. The P_t and polar angle distributions include all tracks in the events. The error bars represent statistical errors only. All distributions are normalized to unity.

$E_{\gamma}^{\rm max}/E_{\rm beam}$ suppress hadronic events produced via initial-state radiation and thus reduce the uncertainty of radiative corrections. The total calorimeter energy $E_{\rm cal}$ is defined as a sum of the energies of all clusters in the electromagnetic calorimeter. The requirement on it suppresses background from cosmic rays whereas the condition on the ratio of the Fox–Wolfram moments H_2/H_0 [34] is efficient for suppression of the $e^+e^- \to l^+l^-(\gamma)$ $(l = e, \mu, \tau)$ background, that of cosmic rays and some kinds of the machine background. The background from two-photon and beam-gas events is suppressed by the requirement on the ratio $|P_{\rm z}^{\rm miss}/E_{\rm obs}|$, where $P_{\rm z}^{\rm miss}$ is the z component of the missing momentum. The background from beam-gas events was also suppressed by the condition on the ratio $E_{\rm LKr}/E_{\rm cal}$ of the energy deposited in the LKr calorimeter and total calorimeter energy. The event vertex position $Z_{\rm vertex}$ is the average of the z_0's of the charged tracks. The condition on $|Z_{\rm vertex}|$ suppresses the background due to beam-gas, beam-wall and cosmic rays.

Table 5
Detection efficiency for the uds continuum in % (statistical errors only).

Point	ε_{JETSET}	ε_{LUARLW}	$\delta\varepsilon/\varepsilon$
1	76.91 ± 0.13	76.77 ± 0.13	-0.2 ± 0.2
2	76.77 ± 0.13	76.95 ± 0.13	$+0.2 \pm 0.2$
3	77.09 ± 0.13	76.96 ± 0.13	-0.2 ± 0.2
4	79.22 ± 0.13	80.11 ± 0.13	-1.1 ± 0.2
5	80.38 ± 0.13	80.34 ± 0.13	-0.0 ± 0.2
6	80.47 ± 0.13	79.98 ± 0.13	-0.6 ± 0.2
7	80.56 ± 0.13	80.73 ± 0.13	$+0.2 \pm 0.2$
8	84.03 ± 0.12	83.84 ± 0.12	-0.2 ± 0.2

In addition, the cosmic background is suppressed with the time-of-flight condition and the muon system veto in the cases when more than two tracks did not cross the interaction region.

By applying the selection criteria for hadronic events described above, we determined the detection efficiencies for eight data points at which the quantity $R_{\rm uds}$ was measured. These values were obtained by using two versions of event simulation and are listed in Table 5. The detection efficiency at point 8 increased drastically mainly due to repairing a significant number of calorimeter channels.

3.4. Luminosity determination

The integrated luminosity at each point was determined by using Bhabha events detected in the LKr calorimeter in the polar angle range $44^\circ < \theta < 136^\circ$. The criteria for e^+e^- event selection are listed below:

- two clusters, each with the energy above 20% of the beam energy;
- acollinearities of the polar $\delta\theta$ and azimuthal $\delta\phi$ angles are less than 18°;
- the total energy of these two clusters exceeds the single beam energy;
- the calorimeter energy not associated with these two clusters does not exceed 20% of the total one;
- the ratio of the Fox–Wolfram moments $H_2/H_0 > 0.6$.

To reject the background from $e^+e^- \to \gamma\gamma$, $e^+e^- \to e^+e^-e^+e^-$ and $e^+e^- \to$ *hadrons* at least one but not more than three tracks originating from the interaction region were required.

3.5. Background processes

To determine the $R_{\rm uds}$ values, we took into account the lepton pair production from the QED processes $e^+e^- \to e^+e^-$, $e^+e^- \to \mu^+\mu^-$ and $e^+e^- \to \tau^+\tau^-$ which are summarized in Table 6.

The contributions of two-photon interactions were studied based on the simulation of $e^+e^- \to e^+e^-X$ events. We found that the contribution of two-photon events to the continuum cross section grows from 0.47% at 3.077 GeV to 0.51% at 3.72 GeV. The estimated uncertainty in the $R_{\rm uds}$ value due to this contribution is less than 0.2%.

3.6. Correction for residual machine background

Our estimates of the contributions of the residual machine background to the observed hadronic cross section at different energy points are listed in the column marked “Method 1” of Table 7. These values were obtained by using runs with separated e^+ and e^- bunches, which were recorded at each energy point.

The number of events which passed selection criteria in the background runs was used to evaluate the residual background under the assumption that the background rate is proportional to the beam current and the measured vacuum pressure.

Table 6
The contribution of the lepton pair production to the observed cross section in %.

Point	Process		
	e^+e^-	$\mu^+\mu^-$	$\tau^+\tau^-$
1	5.06 ± 0.24	1.29 ± 0.27	
2	1.67 ± 0.09	0.42 ± 0.12	
3	3.34 ± 0.17	0.72 ± 0.19	
4	4.03 ± 0.19	0.72 ± 0.15	
5	4.01 ± 0.20	0.69 ± 0.16	
6	3.42 ± 0.19	0.49 ± 0.16	
7	4.14 ± 0.21	0.53 ± 0.15	3.37 ± 0.17
8	2.34 ± 0.13	0.33 ± 0.11	4.05 ± 0.20

Table 7
The residual machine background in % of the observed cross section.

Point	Background in % (statistical errors only)	
	Method 1	Method 2
1	1.35 ± 0.27	1.29 ± 0.27
2	0.65 ± 0.14	0.80 ± 0.15
3	0.81 ± 0.20	0.86 ± 0.21
4	3.80 ± 0.35	4.08 ± 0.36
5	2.33 ± 0.30	2.19 ± 0.29
6	1.09 ± 0.23	1.15 ± 0.24
7	0.75 ± 0.17	0.76 ± 0.18
8	1.82 ± 0.25	1.94 ± 0.26

As a cross check, we assumed that the background rate is proportional to the current only. The results are presented in the last column of Table 7, which is marked as “Method 2”. The maximal difference of 0.28% between the numbers of background events obtained with these two alternatives was considered as an estimate of the corresponding systematic uncertainty.

3.7. Radiative correction

Numerical calculation of the radiative correction factor was performed according to Eq. (1) by using the compilation of the vacuum polarization data by the CMD-2 group [35] and the relation between $R(s)$ and the hadronic part of the vacuum polarization $\Pi_{\rm hadr}(s)$:

$$R(s) = -\frac{3}{\alpha}\,\mathrm{Im}\,\Pi_{\rm hadr}(s). \qquad (2)$$

To obtain the quantity $\tilde{R}$ and the operator $\tilde{\Pi}$ for Eq. (1) the contribution of the J/ψ and $\psi(2S)$ was subtracted analytically from the vacuum polarization data.

The uds continuum below 3.077 GeV was simulated with the LUARLW generator, that allows us to determine the detection efficiency versus the energy radiated in the initial state.

The x dependence of the detection efficiency is shown in Fig. 3.

The radiative correction factors at different center-of-mass energies are listed in Table 8, while the presented systematic uncertainties will be discussed in more detail in Sec. 4.3.

3.8. J/ψ and $\psi(2S)$ contributions

To determine contributions of narrow resonances to the observed cross section we applied resonance parameters retrieved from the fits. The values presented in Table 2 were corrected for the presence of ISR photons. The corrections were obtained via simulation of J/ψ and $\psi(2S)$ hadronic decays at each energy point.

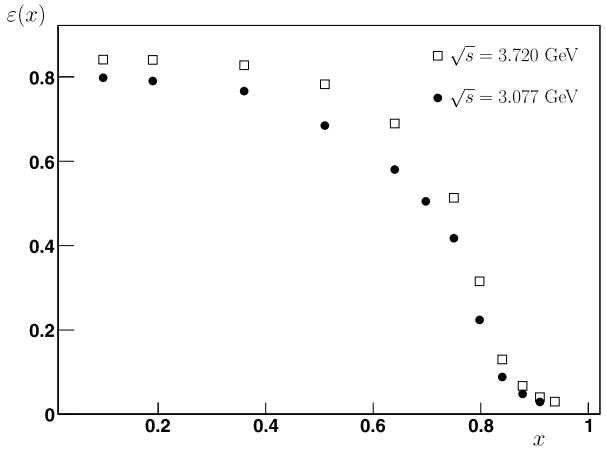

Fig. 3. Hadronic detection efficiency versus the variable x of Eq. (1) at 3.077 GeV and 3.72 GeV.

Table 8
Radiative correction factor $1+\delta$.

Point	$1+\delta$
1	1.1091 ± 0.0089
2	1.1108 ± 0.0089
3	1.1120 ± 0.0056
4	1.1130 ± 0.0078
5	1.1133 ± 0.0067
6	1.1151 ± 0.0056
7	1.1139 ± 0.0078
8	1.1137 ± 0.0056

Table 9
Resulting $R_{\rm uds}$ values with their statistical errors.

Point	$R_{\rm uds}$
1	2.188 ± 0.056
2	2.211 ± 0.046
3	2.214 ± 0.055
4	2.233 ± 0.044
5	2.197 ± 0.047
6	2.224 ± 0.054
7	2.220 ± 0.049
8	2.213 ± 0.047

The detection efficiencies obtained from simulation of hadronic decays in vicinity of narrow resonances are $(79.00 \pm 0.06)\%$ and $(81.40 \pm 0.08)\%$ for J/ψ and $\psi(2S)$, respectively. For both resonances the detection efficiencies obtained by simulation agree with the fit results within the estimated errors.

3.9. Results of energy scan

The results of the $R_{\rm uds}$ measurement obtained in the energy scan are presented in Table 9.

4. Systematic uncertainties and results

4.1. Systematic uncertainty of absolute luminosity determination

The dominant contributions to the systematic error of the absolute luminosity determination with the LKr calorimeter are presented in Table 10.

The uncertainty of the theoretical Bhabha cross section was evaluated by comparing the results obtained with the BHWIDE [26] and MCGPJ [27] event generators at all energy points. The maximum difference did not exceed 0.4% and agreed with the accuracy quoted by the authors.

Table 10
Systematic uncertainties of the luminosity determination.

Source	Uncertainty, %
Cross section calculation	0.4
Calorimeter response	0.4
Calorimeter alignment	0.2
Polar angle resolution	0.1
Background	0.1
MC statistics	0.1
Variation of cuts	0.7
Sum in quadrature	0.9

The systematic uncertainty related to the imperfect simulation of the calorimeter response is about 0.4%. It was quantified by variation of relevant simulation parameters such as the accuracy of the electronic channel calibration, the geometrical factor controlling sensitivity to the energy loss fluctuations between calorimeter electrodes, etc.

The alignment of the tracking system and LKr calorimeter is obtained by reconstructing cosmic rays. By using the primary-vertex distribution of multihadronic and Bhabha events we determined the interaction point position and direction of the beam line. The luminosity uncertainty due to inaccuracy of the alignment is about 0.2%.

The uncertainty related to the difference of the polar angle resolution in simulation and data because of event migration into or out of the fiducial volume is less than 0.1%.

The background to Bhabha events from the processes $e^+e^- \to \mu\mu(\gamma)$ and $e^+e^- \to \gamma\gamma$ and J/ψ and $\psi(2S)$ decays contributes less than 0.2% to the observed e^+e^- cross section at eight energy points listed in Table 1. It was estimated using MC simulation. At the complementary points of the scan used for the determination of the J/ψ and $\psi(2S)$ parameters the contributions of the resonance decays to e^+e^- were calculated by the fitting.

The luminosity uncertainty due to the residual machine background does not exceed 0.1%.

In addition, we varied requirements within the fiducial region to evaluate the effect of other possible sources of a systematic uncertainty. The conditions on the polar angle were varied in a range much larger than the angular resolution, the variation in the Bhabha event count reaches 50%. The requirement on the deposited energy was varied in the range of 70–90% of the c.m. energy. The sum in quadrature of all errors obtained by variation of the selection criteria is about 0.7% and gives an additional estimate of the systematic uncertainty. Despite possible double counting we add this error to the total luminosity uncertainty to obtain a conservative error estimate.

4.2. Uncertainty due to imperfect simulation of continuum

The systematic uncertainty in the $R_{\rm uds}$ value associated with imperfect simulation of the uds continuum was evaluated by using two different MC simulation models. We considered the detection efficiencies at eight energy points reported in Table 5 obtained with the JETSET and LUARLW hadronic generators. It does not exceed a value of 1.1% which was taken as the systematic uncertainty related to the detection efficiency. This estimate is consistent with our previous result of 1.3% obtained in Ref. [15] and agrees with a value of 0.6% found by the variation of selection criteria in Sec. 4.4

Table 11
Systematic uncertainties of the radiative correction.

Point	Uncertainty, %				
	Contributions				Total
	Π approx.	$\delta R_{\rm uds}(s)$	$\delta\varepsilon(s)$	δ_{calc}	
1	0.7	0.2	0.4	0.1	0.8
2	0.7	0.1	0.4	0.1	0.8
3	0.2	0.1	0.4	0.1	0.5
4	0.5	0.1	0.4	0.1	0.7
5	0.4	0.1	0.4	0.1	0.6
6	0.2	0.1	0.4	0.1	0.5
7	0.5	0.1	0.4	0.1	0.7
8	0.1	0.2	0.4	0.1	0.5

4.3. Systematic uncertainty of the radiative correction

The major sources of systematic uncertainty in the radiative correction factor at each energy point are presented in Table 11.

To evaluate the uncertainty related to a choice of the vacuum polarization operator, two alternatives are compared. The first one was taken from the CMD-2 work [35], the second was obtained from the BES event generator [32]. The difference in the results obtained according to the data of the used variants reaches 0.8% at the points closest to J/ψ and varied from 0.1% to 0.5% at the other points.

The contribution denoted as $\delta R_{\rm uds}(s)$ is associated with the $R_{\rm uds}(s)$ uncertainty. It is less than 0.2% for the entire energy range. The contribution $\delta\varepsilon(s)$ of about 0.4% is related to the uncertainty in the $\varepsilon(s)$ dependence. A calculation of the radiative corrections according to Eq. (1) requires the interpolation of the detection efficiency presented in Fig. 3 as a function of x. The contribution $\delta_{\rm calc}$ is related to the interpolation uncertainty. It was estimated by comparing the results obtained using the linear interpolation and the quadratic one.

4.4. Detector-related uncertainties in R_{uds}

The track reconstruction efficiency was studied by using Bhabha events and low-momentum cosmic tracks and the appropriate correction was introduced in the MC simulation. The uncertainty of the correction introduces an additional systematic uncertainty of about 0.2%. We also used two methods to achieve data and MC consistency in the momentum and angular resolution. The first way was to scale the spatial resolution of the drift chamber, while the second method assumed scaling systematic uncertainties of the calibration parameters of the tracking system. The maximal obtained variation of the detection efficiency at various energies is less than 0.3%. Thus, the uncertainty related to track reconstruction is about 0.4%.

The trigger efficiency uncertainty is about 0.2% and mainly comes from the calorimeter thresholds in the secondary trigger. It was estimated by varying the threshold in the software event filter.

The trigger and event selection efficiency depend on the calorimeter response to hadrons. We estimated the uncertainty of 0.2% related to the simulation of nuclear interaction by comparing the efficiencies obtained with the packages GHEISHA [36] and FLUKA [37] which are implemented in GEANT 3.21 [23].

The effect of other possible sources of the detector-related uncertainty was evaluated by varying the event selection criteria that are presented in Table 12. Tightening of some requirements listed in Table 12 by several times varies a contribution to the observed cross section of physical and machine background events and significantly changes the detection efficiency. That allows us to verify uncertainties associated with the background and radiative corrections.

Table 12
$R_{\rm uds}$ uncertainty due to variation of the selection criteria for hadronic events.

Condition/variable	Range variation	$R_{\rm uds}$ variation in %
$N_{\rm particles} \geq 3$ OR $\tilde{N}^{\rm IP}_{\rm track} \geq 2$	$N_{\rm particles} \geq 4$ OR $\tilde{N}^{\rm IP}_{\rm track} \geq 2$	0.1
$N^{\rm IP}_{\rm track}$	≥ 1 OR no cut	0.1
$E_{\rm obs}$	$> 1.4 \div 1.8$ GeV	0.3
$E^{\rm max}_{\gamma}/E_{\rm beam}$	$< 0.6 \div 0.9$	0.3
$E_{\rm cal}$	$> 0.5 \div 0.75$ GeV	0.2
H_2/H_0	$< 0.7 \div 0.93$	0.2
$\lvert P^{\rm miss}_z/E_{\rm obs}\rvert$	$< 0.6 \div 0.8$	0.2
$E_{\rm LKr}/E_{\rm cal}$	$> 0.15 \div 0.25$	0.1
$\lvert Z_{\rm vertex}\rvert$	$< 20.0 \div 13.0$ cm	0.2
Sum in quadrature		0.6

Table 13
$R_{\rm uds}$ systematic uncertainties in % assigned to each energy point.

	1	2	3	4	5	6	7	8
Luminosity	0.9	0.9	0.9	0.9	0.9	0.9	0.9	0.9
Radiative correction	0.8	0.8	0.5	0.7	0.6	0.5	0.7	0.5
Continuum simulation	1.1	1.1	1.1	1.1	1.1	1.1	1.1	1.1
Track reconstruction	0.4	0.4	0.4	0.4	0.4	0.4	0.4	0.4
e^+e^-X contribution	0.2	0.2	0.2	0.2	0.2	0.2	0.2	0.2
l^+l^- contribution	0.4	0.4	0.4	0.3	0.3	0.3	0.4	0.4
Trigger efficiency	0.2	0.2	0.2	0.2	0.2	0.2	0.2	0.2
Nuclear interaction	0.2	0.2	0.2	0.2	0.2	0.2	0.2	0.2
Cuts variation	0.6	0.6	0.6	0.6	0.6	0.6	0.6	0.6
J/ψ and $\psi(2S)$	0.1	1.8	0.4	0.2	0.1	0.1	0.1	1.1
Machine background	0.4	0.8	0.5	0.6	0.5	0.4	0.4	0.6
Sum in quadrature	1.9	2.7	1.9	1.9	1.8	1.8	1.9	2.2

Table 14
Correlated systematic uncertainties $R_{\rm uds}$ in % for data of 2011 and 2014.

Source	Uncertainty in %
Luminosity	
Cross section calculation	0.4
Radiative correction	
Π approx.	$0.1 \div 0.3$
$\delta R_{\rm uds}(s)$	$0.1 \div 0.2$
$\delta\varepsilon(s)$	0.2
Continuum simulation	0.9
e^+e^-X contribution	0.1
l^+l^- contribution	0.2
Trigger efficiency	0.2
Nuclear interaction	0.2
Sum in quadrature	1.1

All observed $R_{\rm uds}$ variations were smaller than their statistical errors and can originate from the already considered sources of uncertainties or statistical fluctuations. By keeping a conservative estimate, we added them in the total uncertainty.

4.5. Summary of systematic uncertainties and results

The major sources of the systematic uncertainty on the $R_{\rm uds}$ value are listed in Table 13.

During data collection at a given energy point the relative beam energy variation was less than 10^{-3} allowing us to neglect this source of uncertainty.

The results obtained at most points supplement the data published in Ref. [15]. In order to use these data in the calculations of the dispersion integrals it is important to combine results of both

Table 15
Measured values of $R_{\rm uds}(s)$ and $R(s)$ with statistical and systematic uncertainties.

Data 2011 [15]		Data 2014		Combination	
$\sqrt{s}$, MeV	$R_{\rm uds}(s)$	$\sqrt{s}$, MeV	$R_{\rm uds}(s)$	$\sqrt{s}$, MeV	$R_{\rm uds}(s)\{R(s)\}$
–	–	3076.7 ± 0.2	$2.188 \pm 0.056 \pm 0.042$	3076.7 ± 0.2	$2.188 \pm 0.056 \pm 0.042$
3119.9 ± 0.2	$2.215 \pm 0.089 \pm 0.066$	3119.2 ± 0.2	$2.211 \pm 0.046 \pm 0.060$	3119.6 ± 0.4	$2.212\{2.235\} \pm 0.042 \pm 0.049$
3223.0 ± 0.6	$2.172 \pm 0.057 \pm 0.045$	3221.8 ± 0.2	$2.214 \pm 0.055 \pm 0.042$	3222.5 ± 0.8	$2.194\{2.195\} \pm 0.040 \pm 0.035$
3314.7 ± 0.7	$2.200 \pm 0.056 \pm 0.043$	3314.7 ± 0.4	$2.233 \pm 0.044 \pm 0.042$	3314.7 ± 0.6	$2.219\{2.219\} \pm 0.035 \pm 0.035$
3418.2 ± 0.2	$2.168 \pm 0.050 \pm 0.042$	3418.3 ± 0.4	$2.197 \pm 0.047 \pm 0.040$	3418.3 ± 0.3	$2.185\{2.185\} \pm 0.032 \pm 0.035$
–	–	3499.6 ± 0.4	$2.224 \pm 0.054 \pm 0.040$	3499.6 ± 0.4	$2.224\{2.224\} \pm 0.054 \pm 0.040$
3520.8 ± 0.4	$2.200 \pm 0.050 \pm 0.044$	–	–	3520.8 ± 0.4	$2.200\{2.201\} \pm 0.050 \pm 0.044$
3618.2 ± 1.0	$2.201 \pm 0.059 \pm 0.044$	3618.1 ± 0.4	$2.220 \pm 0.049 \pm 0.042$	3618.2 ± 0.7	$2.212\{2.218\} \pm 0.038 \pm 0.035$
3719.4 ± 0.7	$2.187 \pm 0.068 \pm 0.060$	3719.6 ± 0.2	$2.213 \pm 0.047 \pm 0.049$	3719.5 ± 0.5	$2.204\{2.228\} \pm 0.039 \pm 0.042$

experiments by taking into account correlated uncertainties properly. This requires to determine the common components of the uncertainties which are the same for each experiment. The corresponding contributions to the systematic uncertainty are listed in Table 14.

The results of the two scans were averaged using their statistical uncertainties and the uncorrelated parts of the systematic ones. The formal description of the averaging procedure can be found in Ref. [19]. The obtained $R_{\rm uds}$ and R values as well as luminosity-weighted average center-of-mass energies are presented in Table 15. As mentioned above, the contribution of narrow resonances to $R(s)$ is not negligible in the resonance region. This contribution was determined analytically by using "bare" parameters of the resonances, which were calculated based on the PDG data [21]. The inaccuracy of R associated with the resonance parameters is negligible in comparison with the other uncertainties, so the errors for the values of R and $R_{\rm uds}$ are the same.

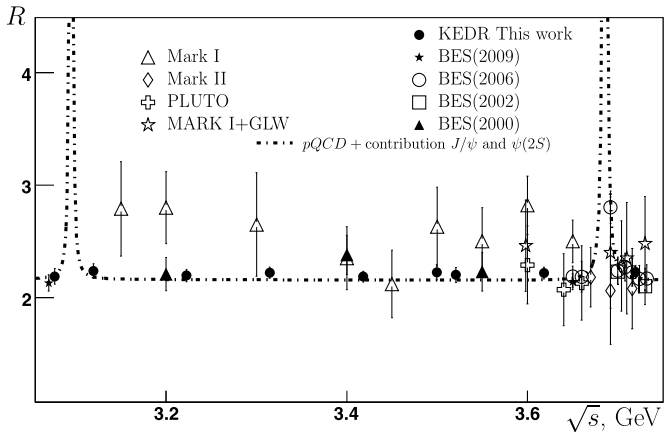

Fig. 4. The quantity R versus the c.m. energy and the sum of the prediction of perturbative QCD and a contribution of narrow resonances.

5. Results

By combining new data with our previous results we determined the values of $R_{\rm uds}$ and R at nine center-of-mass energy points between 3.08 and 3.72 GeV. The accuracy of R measurements in comparison with our previous results [15] was increased by $1.4 \div 1.7$ times. The total error is about or better than 2.6% at most of energy points with a systematic uncertainty of about 1.9%. This result provides the most precise information about R in this energy range. The measured R values are shown in Fig. 4. For completeness, we remind that in the R measurement performed at KEDR in the c.m. energy range 1.84–3.05 GeV the total uncertainty was 3.9% or better with a systematic one of about 2.4% [16].

In the c.m. energy range 3.08–3.72 GeV the weighted average $\overline{R}_{\rm uds} = 2.204 \pm 0.014 \pm 0.026$ is approximately one sigma higher than that theoretically expected, $R^{\rm pQCD}_{\rm uds} = 2.16 \pm 0.01$ calculated according to the pQCD expansion [38] for $\alpha_s(m_\tau) = 0.333 \pm 0.013$ obtained from semileptonic τ decays [39]. In the lower c.m. energy range 1.84–3.05 GeV the weighted average is $2.225 \pm 0.020 \pm 0.047$ in good agreement with the pQCD prediction of 2.18 ± 0.02.

It should be noted that while calculating the dispersion integrals in this energy range it is preferable to use the measured $R_{\rm uds}(s)$ values by adding the contribution of narrow resonances calculated analytically. This approach prevents from a possible double counting of the contribution of narrow resonances.

Table 16
Summary table of KEDR results. Actual energies and measured R values.

Point	Energy	$R_{\rm uds}(s)\{R(s)\}$
Data 2010 [16]		
1	1841.0 ± 2	$2.226 \pm 0.139 \pm 0.158$
2	1937.0 ± 2	$2.141 \pm 0.081 \pm 0.073$
3	2037.3 ± 2	$2.238 \pm 0.068 \pm 0.072$
4	2135.7 ± 2	$2.275 \pm 0.072 \pm 0.055$
5	2239.2 ± 2	$2.208 \pm 0.069 \pm 0.053$
6	2339.5 ± 2	$2.194 \pm 0.064 \pm 0.048$
7	2444.1 ± 2	$2.175 \pm 0.067 \pm 0.048$
8	2542.6 ± 2	$2.222 \pm 0.070 \pm 0.047$
9	2644.8 ± 2	$2.220 \pm 0.069 \pm 0.049$
10	2744.6 ± 2	$2.269 \pm 0.065 \pm 0.050$
11	2849.7 ± 2	$2.223 \pm 0.065 \pm 0.047$
12	2948.9 ± 2	$2.234 \pm 0.064 \pm 0.051$
13	3048.1 ± 2	$2.278 \pm 0.075 \pm 0.048$
Combined Data 2011 [15] and 2014 (this work)		
14	3076.7 ± 0.2	$2.188 \pm 0.056 \pm 0.042$
15	3119.6 ± 0.4	$2.212\{2.235\} \pm 0.042 \pm 0.049$
16	3222.5 ± 0.8	$2.194\{2.195\} \pm 0.040 \pm 0.035$
17	3314.7 ± 0.6	$2.219\{2.219\} \pm 0.035 \pm 0.035$
18	3418.3 ± 0.3	$2.185\{2.185\} \pm 0.032 \pm 0.035$
19	3499.6 ± 0.4	$2.224\{2.224\} \pm 0.054 \pm 0.040$
20	3520.8 ± 0.4	$2.200\{2.201\} \pm 0.050 \pm 0.044$
21	3618.2 ± 1.0	$2.212\{2.218\} \pm 0.038 \pm 0.035$
22	3719.4 ± 0.7	$2.204\{2.228\} \pm 0.039 \pm 0.042$

6. Summary and applications

Together with the high-precision R measurement below the J/ψ [16], KEDR measured the R values at twenty two center-of-mass energies between 1.84 and 3.72 GeV listed in Table 16.

To use $R(s)$ data it is necessary to take into account point-by-point correlated effects. The analysis of the sources of systematic uncertainties makes it possible to identify common contributions in the listed data sets. Similarly to the Table 14 presented above, the correlated systematic uncertainties $R_{\rm uds}$ for other data sets are listed in Table 17. Keeping a conservative approach, we believe these contributions are completely correlated, that allows us to write down an approximate correlation matrix for systematic un-

Table 17
Correlated systematic uncertainties of $R_{\rm uds}$ in % for data of 2010, 2011 and 2014.

Source	Uncertainty in %	
	Data 2010	Data 2010/Data 2011, 2014
Luminosity		
Cross section calc.	0.5	0.4
Calorimeter response	0.7	–
Calorimeter alignment	0.2	0.2
Radiative correction		
Π approx.	0.3	0.1
$\delta R_{\rm uds}(s)$	0.2	0.2
$\delta\varepsilon(s)$	0.3	0.2
Continuum simulation	1.2	$0.4 \div 0.8$
Track reconstruction	0.5	0.4
e^+e^-X contribution	0.2	0.1
l^+l^- contribution	0.3	0.2
Trigger efficiency	0.3	0.2
Nuclear interaction	0.4	0.2
Sum in quadrature	1.8	$0.8 \div 1.1$

certainties (Table 18). Note that statistical errors in our R results are fully uncorrelated.

The determination of the R ratio plays a key role in the determination of the running strong coupling constant $\alpha_s(s)$. To verify the compatibility with other measurements of $\alpha_s(s)$ we performed a fit of $R_{\rm uds}$ in the given energy range using the following approximation [38]:

$$R^{\rm calc}_{\rm uds}(s) = 2 \times \left(1 + \frac{\alpha_s}{\pi} + \frac{\alpha_s^2}{\pi^2} \times \left(\frac{365}{24} - 9\zeta_3 - \frac{11}{4}\right)\right), \tag{3}$$

where ζ is the Euler–Riemann zeta function and $\alpha_s(s)$ is approximated by:

$$\alpha_s(s) = \frac{1}{b_0 t}\left(1 - \frac{b_1 l}{b_0^2 t} + \frac{b_1(l^2 - l - 1) + b_0 b_2}{b_0^4 t^2} + \frac{b_1^3(-2l^3 + 5l^2 + 4l - 1) - 6b_0 b_2 b_1 l + b_0^2 b^3}{2b_0^6 t^3}\right), \tag{4}$$

with $t = \ln\frac{s}{\Lambda^2}$, $l = \ln t$ parametrized in terms of the QCD scale parameter Λ and coefficients b_0, b_1, b_3 defined in [40].

To determine Λ, we minimise the χ^2 function

$$\chi^2 = \sum_i \sum_j \left(R^{\rm meas}_{\rm uds}(s_i) - R^{\rm calc}_{\rm uds}(s_i)\right) C^{-1}_{ij} \left(R^{\rm meas}_{uds}(s_j) - R^{\rm calc}_{\rm uds}(s_j)\right), \tag{5}$$

where C^{-1}_{ij} are coefficients of the inverse covariance matrix which is derived from statistical errors and systematic uncertainties taking into account the correlation matrix presented in Table 18.

The obtained value of $\Lambda = 0.361^{+0.155}_{-0.174}$ GeV corresponds to $\alpha_s(m_\tau) = 0.332^{+0.100}_{-0.092}$. If the next order of pQCD is included in the expansion of $R_{\rm uds}$, the fitting results are as follows: $\Lambda = 0.437^{+0.210}_{-0.215}$ GeV and $\alpha_s(m_\tau) = 0.378^{+0.173}_{-0.120}$. So, we can conclude that our measurements of $R(s)$ are consistent with the pQCD predictions within their errors.

Another practical application of the $R(s)$ measurement is related to determination of the heavy quark masses. This calculation is based on sum rules and experimental moments $M_n^{\rm exp}$, which are defined as follows:

$$M_n^{\rm exp} = \int \frac{R(s)}{s^{n+1}} ds\,. \tag{6}$$

Table 18
The correlation matrix for systematic uncertainties of the R values obtained in the KEDR experiments.

Point	Correlation matrix																					
1	1	0.139	0.143	0.193	0.192	0.212	0.212	0.216	0.207	0.211	0.216	0.201	0.222	0.096	0.046	0.096	0.105	0.110	0.098	0.089	0.114	0.071
2		1	0.309	0.418	0.408	0.445	0.437	0.466	0.446	0.457	0.467	0.434	0.480	0.200	0.097	0.201	0.225	0.229	0.212	0.189	0.244	0.151
3			1	0.423	0.425	0.470	0.470	0.480	0.460	0.463	0.480	0.442	0.486	0.212	0.101	0.212	0.232	0.243	0.218	0.198	0.253	0.158
4				1	0.575	0.635	0.635	0.649	0.622	0.610	0.649	0.598	0.637	0.287	0.137	0.286	0.314	0.329	0.295	0.268	0.342	0.213
5					1	0.621	0.621	0.642	0.615	0.629	0.643	0.598	0.661	0.280	0.134	0.280	0.310	0.322	0.293	0.262	0.336	0.208
6						1	0.677	0.709	0.679	0.695	0.710	0.661	0.730	0.306	0.148	0.305	0.342	0.351	0.323	0.287	0.371	0.229
7							1	0.709	0.679	0.695	0.710	0.661	0.730	0.304	0.148	0.305	0.342	0.348	0.323	0.287	0.371	0.229
8								1	0.695	0.710	0.725	0.675	0.745	0.320	0.153	0.320	0.351	0.368	0.330	0.299	0.382	0.238
9									1	0.681	0.695	0.647	0.715	0.307	0.146	0.306	0.336	0.352	0.316	0.287	0.366	0.228
10										1	0.710	0.654	0.701	0.314	0.150	0.313	0.344	0.360	0.323	0.293	0.374	0.233
11											1	0.675	0.745	0.321	0.153	0.320	0.351	0.368	0.330	0.300	0.382	0.238
12												1	0.687	0.298	0.142	0.298	0.327	0.342	0.307	0.279	0.356	0.222
13													1	0.330	0.157	0.329	0.361	0.378	0.339	0.308	0.393	0.245
14														1	0.288	0.396	0.405	0.394	0.356	0.317	0.403	0.333
15															1	0.345	0.347	0.345	0.305	0.275	0.345	0.288
16																1	0.486	0.475	0.427	0.38	0.483	0.400
17																	1	0.486	0.427	0.387	0.486	0.405
18																		1	0.427	0.38	0.483	0.400
19																			1	0.340	0.427	0.356
20																				1	0.384	0.318
21																					1	0.403
22																						1

The inclusion in the analysis of our new results increases the accuracy of the contribution of light quarks to experimental moments by almost two times in the given energy range. According to Ref. [41], the total uncertainty of c quark mass determination is 8 MeV, in which the light quark contribution is about 2 MeV. By applying new KEDR results one can reduce this contribution down to 1 MeV.

Acknowledgements

We greatly appreciate the efforts of the staff of VEPP-4M to provide good operation of the complex during long term experiments. The authors are grateful to V. P. Druzhinin for useful discussions. The Siberian Branch of the Russian Academy of Sciences Siberian Supercomputer Center and Novosibirsk State University Supercomputer Center are gratefully acknowledged for providing supercomputer facilities.

This work has been supported by Russian Science Foundation (project N 14-50-00080). SE acknowledges Russian Science Foundation (project N 17-12-01036) for supporting part of this work related to Monte Carlo generators.

References

[1] M. Davier, et al., Eur. Phys. J. C 71 (2011) 1515.
[2] K. Hagiwara, et al., J. Phys. J. G 38 (2011) 085003.
[3] N. Brambilla, et al., Eur. Phys. J. C 71 (2011) 1534.
[4] M. Grilli, et al., Nuovo Cimento Lett. A 13 (1973) 593.
[5] P.A. Rapidis, et al., Phys. Rev. Lett. 39 (1977) 526.
[6] J. Burmester, et al., Phys. Lett. B 66 (1977) 395.
[7] C. Bacci, et al., Phys. Lett. B 86 (1979) 234.
[8] R.H. Schindler, et al., Phys. Rev. D 21 (1980) 2716.
[9] B. Esposito, et al., Nuovo Cimento Lett. 30 (1981) 65.
[10] J.L. Siegrist, et al., Phys. Lett. B 26 (1982) 969.
[11] J.Z. Bai, et al., BES Collaboration, Phys. Rev. Lett. 84 (2000) 594.
[12] J.Z. Bai, et al., BES Collaboration, Phys. Rev. Lett. 88 (2002) 101802.
[13] M. Ablikim, et al., BES Collaboration, Phys. Rev. Lett. 97 (2006) 262001.
[14] M. Ablikim, et al., BES Collaboration, Phys. Lett. B 677 (2009) 239.
[15] V.V. Anashin, et al., KEDR Collaboration, Phys. Lett. B 753 (2016) 533.
[16] V.V. Anashin, et al., KEDR Collaboration, Phys. Lett. B 770 (2017) 174.
[17] V.V. Anashin, et al., in: EPAC 98*, Stockholm 1998, 1998, p. 400.
[18] V.V. Anashin, et al., KEDR Collaboration, Phys. Part. Nucl. 44 (2013) 657.
[19] V.V. Anashin, et al., KEDR Collaboration, Phys. Lett. B 711 (2012) 280.
[20] V.V. Anashin, et al., KEDR Collaboration, Phys. Lett. B 749 (2015) 50.
[21] K.A. Olive, et al., PDG, Chin. Phys. C 38 (2014) 090001.
[22] E.A. Kuraev, V.S. Fadin, Sov. J. Nucl. Phys. 41 (1985) 466.
[23] GEANT – Detector Description and Simulation Tool, CERN Program Library Long Writeup W5013.
[24] T. Sjostrand, M. Bengtsson, Comput. Phys. Commun. 43 (1987) 367.
[25] Haiming Hu, An Tai, eConf C010430, T24, arXiv:hep-ex/0106017, 2001.
[26] S. Jadach, W. Placzek, B.F.L. Ward, Phys. Lett. B 390 (1997) 298.
[27] A.B. Arbuzov, et al., Eur. Phys. J. C 46 (2006) 689.
[28] S. Jadach, Z. Was, Comput. Phys. Commun. 85 (1995) 453.
[29] F.A. Berends, et al., Comput. Phys. Commun. 40 (1986) 285.
[30] F.A. Berends, et al., Comput. Phys. Commun. 40 (1986) 271.
[31] V.A. Tayursky, S.I. Eidelman, Preprint IYaF 2000-78, Novosibirsk, 2000 (in Russian).
[32] J.C. Chen, et al., Phys. Rev. D 62 (2000) 034003.
[33] V.V. Anashin, et al., KEDR Collaboration, J. High Energy Phys. 1805 (2018) 119, arXiv:1801.01958.
[34] G.C. Fox, S. Wolfram, Nucl. Phys. B 149 (1979) 413.
[35] S. Actis, et al., Eur. Phys. J. C 66 (2010) 585.
[36] H.C. Fesefeldt, Technical Report PITHA-85-02, III Physilakisches Institut, RWTH Aachen Physikzentrum, 5100 Aachen, Germany, Sep. 1985.
[37] A. Fassò, et al., Talk at the Computing in High Energy and Nuclear Physics (CHEP03), arXiv:physics/0306162.
[38] P.A. Baikov, et al., Phys. Lett. B 714 (2012) 62.
[39] N. Brambilla, et al., Eur. Phys. J. C 74 (2014) 2981.
[40] M. Tanabashi, et al., (PDG), Phys. Rev. D 98 (2018) 030001.
[41] J. Erler, P. Masjuan, H. Spiesberger, Mod. Phys. Lett. A 31 (2016) 1630041, arXiv:1611.05648.